ACS ENGINEERING Au
AN OPEN ACCESS JOURNAL OF THE AMERICAN CHEMICAL SOCIETY

pubs.acs.org/engineeringau
Article

Interplay of Spatial and Topological Defects in Polymer Networks

Published as part of ACS Engineering Au virtual special issue "Materials Design".

B. Ruşen Argun and Antonia Statt*

Cite This: *ACS Eng. Au* 2024, 4, 351−358
Read Online

ABSTRACT: Polymer networks are widely used in applications, and the formation of a network and its gel point can be predicted. However, the effects of spatial and topological heterogeneity on the resulting network structure and ultimately the mechanical properties, are less understood. To address this challenge, we generate in silico random networks of cross-linked polymer chains with controlled spatial and topological defects. While all fully reacted networks investigated in this study have the same number of end-functionalized polymer strands and cross-linkers, we vary the degree of spatial and topological heterogeneities systematically. We find that spatially heterogeneous cross-linker distributions result in a reduction in the network's primary loops with increased spatial heterogeneity, the opposite trend as observed in homogeneous networks. By performing molecular dynamics simulations, we investigated the mechanical properties of the networks. Even though spatially heterogeneous networks have more elastically active strands and cross-linkers, they break at lower extensions than the homogeneous networks and sustain slightly lower maximum stresses. Their shear moduli are higher, i.e., stiffer, than theoretically predicted, and higher than their homogeneous gel counterparts. Our results highlight that topological loop defects and spatial heterogeneities result in significantly different network structures and, ultimately, different mechanical properties.

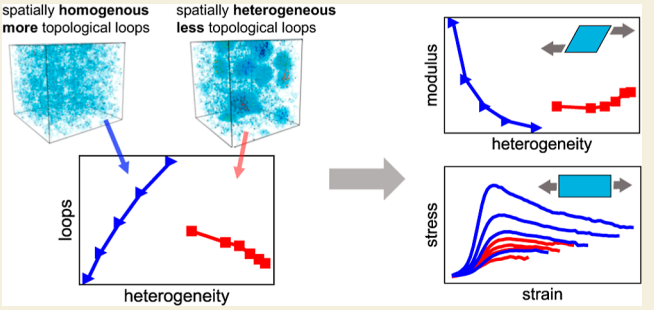

KEYWORDS: *cross-linked polymers, thermosets, molecular dynamics simulations, network structure, gelation, polymer network elasticity*

1. INTRODUCTION

Polymer networks and gels[1,2] find widespread applications as both commodity materials and specialized functional materials in biomedical applications,[3] or stimulus-responsive materials.[4] While various theories exist to describe the formation of these networks,[5−13] classical models often assume idealized conditions and structures without accounting for topological defects, e.g., loops, dangling ends, or spatial heterogeneities, e.g., concentration fluctuations. In reality, factors such as chemical composition variations, nonideal mixing, and polymerization schemes,[1,14−17] introduce complex heterogeneities that impact gelation and final network structure.[17−19] Topological defects formed during cross-linking can actually lead to spatial heterogeneities.[20] However, characterizing polymer networks experimentally, especially in terms of their topology and spatial distribution, can be challenging, yet it is essential for a fundamental understanding of network properties.[21−23]

While the effect of topological defects like dangling ends, loops, and higher-order loops on the gel point has been investigated recently,[24−27] spatial heterogeneity is typically not considered. Those studies[24−26] have shown that topological defects depend on polymer concentration and increases in loop fraction led to increased gel points. Random networks usually have lower moduli than expected from the targeted molecular weight of their strands, which is commonly attributed to both topological and spatial heterogeneities; however, the relative contributions of each are not fully understood.[23]

Including both spatial and topological heterogeneities in model network structure is important for accurate descriptions of micro and nanogels.[28,29] Additionally, the elasticity and mechanical behavior of networks is inherently related to their molecular network structure.[30−33] While there are examples of computational studies[34,35] which explicitly study heterogeneity effects; however, they did not determine the effect on the gel point. While many computational studies[16,36−39] incorporate topological defects and potentially spatial variations by employing reaction mechanisms to form gels, commonly, the heterogeneous structure of the network is not explicitly controlled or systematically investigated.

Received: November 29, 2023
Revised: February 16, 2024
Accepted: February 20, 2024
Published: March 1, 2024

In this work, we address this gap by modifying the efficient random network algorithm by Gusev[40,41] to explicitly include both spatial concentration fluctuations and topological network defects. By systematically investigating both spatial and topological defects, this study aims to move toward a more comprehensive understanding of the impact of defects on network properties and their mechanical properties.

In the following, we will first describe the algorithm and extension in Section 2. Then, in Section 3 we show that spatially heterogeneous cross-linker distributions reduce primary loop fractions. Despite having more active strands and cross-linkers, spatially heterogeneous networks exhibit lower extension at their break point, need fewer bonds to break for failure, and have slightly lower maximum stresses. Their shear moduli exceed affine network theory (ANT) predictions and those of comparable homogeneous gels; i.e., they are stiffer than expected. In Section 4, we conclude and provide an outlook.

2. METHODS

The gels in this work were obtained by using a custom variation of the random Gaussian network generation algorithm.[40,41] In short, this efficient algorithm creates large-scale polymer networks by sequentially adding polymer strands, ignoring excluded volume effects. First, the cross-linker positions are drawn from a random uniform distribution. Next, strands are added sequentially to cross-linkers with probability ζ and then reacted with a second cross-linker, again with probability ζ. The second cross-linker is randomly selected from the Gaussian distribution of distances of all of the available cross-linkers from the first, already-reacted end. While this algorithm might not entirely reflect the more random, stochastic nature of gel formation in experiments, it allows the generation of realistic Gaussian networks in an extremely computationally efficient manner. A systematic investigation with statistical significance of the effects described here is only possible with an efficient algorithm, as the traditional molecular dynamics approach of modeling the cross-linking reactions explicitly is too slow and lacks systematic control.

In order to enable molecular dynamics simulations with the fully reacted networks, as obtained by this algorithm, all strands must be placed into the system as explicit bead−spring chains. We use Brownian bridges[42] to draw each strand position in between the chosen cross-linker positions. All systems in this study contained N_p = 2000 end-reactive strands of length M = 100 with N_{cr} = 1000 cross-linkers with a functionality f = 4, i.e., at perfect stoichiometric balance. For all networks, a high conversion rate of ζ = 0.99 was used; i.e., almost all chains will be cross-linked to a cluster since the probability of reacting to each end is 99%. All networks were made by iterating over all N_p = 2000 end-reactive strands.

Control over the topological defects and spatial heterogeneities in this algorithm can be achieved by multiple different means. Here, we investigate two distinct ways, first, homogeneously changing the overall density of the system[40,41,43] as done previously, and second, changing the initial spatial distribution of cross-linkers. Lowering the overall density keeps the gel spatially homogeneous and increases the fraction of topological defects, e.g., loops.

For the uniform systems, the primary loop fraction (i.e., polymer strands with both ends connected to the same cross-linker) was varied from approximately 0.11 to 0.3 by changing the box size from $80\sigma \times 80\sigma \times 80\sigma$ up to $120\sigma \times 120\sigma \times 120\sigma$, where σ is a bead diameter and sets the unit of length. Consequently, the overall number density of cross-links changed from $\rho = 0.0006\sigma^{-3}$ to $\rho = 0.002\sigma^{-3}$. As the density of cross-linkers and strands increases, the probability of loop formation decreases, since it is more likely to find a different available cross-linker within the required distance.

The second method of introducing defects is loosely inspired by ref 34 and has not been used with this algorithm before. Here, the overall density of cross-linkers is kept constant (N_{cr} = 1000 cross-linkers in a box of size $100\sigma \times 100\sigma \times 100\sigma$), while the cross-linker distribution is changed from a random uniform distribution to a more and more heterogeneous distribution with larger spatial density variations. While this distribution can take any form, we used ten small spherical regions with approximately a radius of 3σ, where we increased the local cross-linker number density from the average value to up to approximately $0.5\sigma^{-3}$ (most heterogeneous case) in addition to the uniform background distribution. The background density was consequently reduced down to approximately $0.00044\sigma^{-3}$ to keep the overall number density of cross-links constant. Details of the code for the cross-linker distribution and local density histograms are described in the Supporting Information. In the spatially heterogeneous networks, the second virial coefficient as derived from the cross-linker pair correlation distribution is negative, and the monomer density distribution is broader but not bimodal. In the homogeneous networks, the second virial coefficient is slightly positive. Other forms of spatial heterogeneity will be interesting to investigate in the future. Typical snapshots of the resulting networks are shown in Figure 1. Here, we show two networks with very different structural properties. One is spatially homogeneous with about 30% primary loop chains, and the other one has only 13% loop chains but is spatially heterogeneous with denser regions.

We modeled each strand with M = 100 WCA[44−46] beads

$$U_{\mathrm{WCA}}(r) = \begin{cases} 4\epsilon\left[\left(\frac{\sigma}{r}\right)^{12} - \left(\frac{\sigma}{r}\right)^{6} + \frac{1}{4}\right] & \text{if } r < 2^{1/6}\sigma \\ 0 & \text{otherwise} \end{cases} \quad (1)$$

with standard parameters σ = 1.0, ϵ = 1.0 and $r_{\mathrm{cut}} = 2^{1/6}\sigma$. All beads were linked by standard FENE bonds

$$U_{\mathrm{fene}}(r) = -0.5KR_0^2 \ln\left[1 - \left(\frac{r}{R_0}\right)^2\right] + U_{\mathrm{WCA}}(r) \quad (2)$$

with parameters $R_0 = 1.5\sigma$ and $K = 30\epsilon/\sigma^2$. For the deformation, we implemented breakable quartic bonds of shape

$$U_{\mathrm{quartic}}(r) = k(r - r_{cut})^3(r - r_1) \quad (3)$$

with parameters $k = 7497.7427\epsilon/\sigma^4$, $r_{\mathrm{cut}} = 1.3\sigma$, and $r_1 = 0.85866\sigma$.[47,48] These parameters are chosen such that the minimum position is the same as that in U_{fene}. The bond and pair interactions are plotted in the Supporting Information. All gels obtained with the algorithms described above have the same number of cross-linkers and strands, so the properties are directly comparable.

This model represents polymer chains in an athermal solvent. After the replacement, some beads might overlap since the original algorithm does not include excluded volume effects. To remove any overlaps, we performed a FIRE minimization[49] and equilibrated the resulting configurations with a Langevin thermostat at $T = 1.0\epsilon/k_B$ with a time step of δt = 0.005 for 2500τ. An additional NpT at $p \approx 0$ ensemble equilibration was performed for 25000τ after that, which led to moderate swelling of the networks. These simulations were

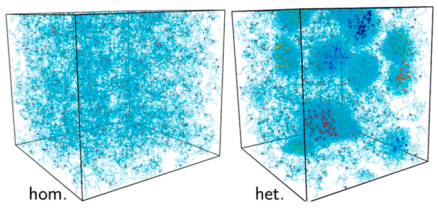

Figure 1. Snapshots of representative equilibrated fully reacted network configurations, where the left shows the most dilute homogeneous case and the right is the most heterogeneous case, with ρ_h values of 1.74 (hom.) and 3.45 (het.). Strands are shown as blue lines, and cross-linkers are shown as larger beads where the color corresponds to the spatial dense region they belong to.

https://doi.org/10.1021/acsengineeringau.3c00072
ACS Eng. Au 2024, 4, 351−358

performed with FENE bonds to avoid the accidental degradation of the network by bond breaking. This implicit solvent swelling ratio is shown in the Supporting Information. All molecular dynamics simulations were performed using the open-source package HOOMD-blue v3[50] with a tree neighbor list[51] for computational efficiency in spatially sparse systems. Once equilibrated, the bond potentials were swapped out for the quartic bonds, and the gels were deformed, either with a simple shear or extensional box deformation. We monitored bond breaking and measured the resulting relaxation and stress−strain curves.

3. RESULTS AND DISCUSSION

To compare different networks, we used a normalized maximum density order parameter, given by

$$\rho_h = \frac{\rho_{max}}{\rho_{av}} - 1 \tag{4}$$

where ρ_{av} is the overall average monomer density in the system, and ρ_{max} is the maximum monomer density observed in any small $6\sigma \times 6\sigma \times 6\sigma$ region of the system. Full-density histograms are displayed in the Supporting Information. This normalized maximum density ρ_h would be equal to zero for a perfectly homogeneous gel with zero density fluctuations and is increasing as the spatial heterogeneity increases. The maximum observed densities were in the range $0.319\sigma^{-3}$ to $0.895\sigma^{-3}$, with average monomer densities of $0.116\sigma^{-3}$ to $0.393\sigma^{-3}$. However, this order parameter does not capture the distribution or exact morphology of the spatial heterogeneity.

As shown in Figure 2, increasing the spatial heterogeneity (i.e. local density fluctuations) in the homogeneous networks is correlated with an increase in topological defects, e.g. primary loops l_1, strands where both ends are connected to the same cross-linker. However, explicit spatial heterogeneity (i.e. dense clusters) in the system decreased the fraction of loop defects. This opposite trend to the homogeneous system can be rationalized by the fact that in the dense regions, it is significantly more likely to find a suitable other cross-linker to connect to, reducing the overall loop defects. At the same time, few key connections in the more dilute regions of the network still need to be established to form a gel.

Topological defects also include higher-order loops, e.g., secondary loops, where two polymer strands are connected to the same two cross-linkers, or tertiary loops, where three strands connect the same three cross-linkers.[33] Figure 3 displays the fraction of these higher-order loop defects, e.g., secondary l_2, tertiary l_3, and quaternary l_4 loops. All topological defects follow the same trend as the primary loop fraction, and their respective amounts decrease as their order increases.

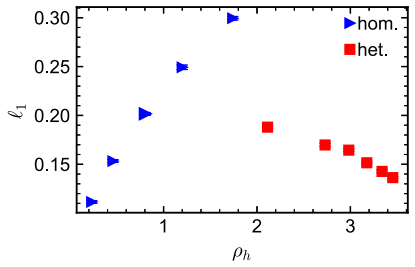

Figure 2. Primary loop fraction l_1 in the fully formed homogeneous (blue) and heterogeneous (red) networks as a function of ρ_h. Each point is an average of 30 independent runs and the error bars indicate the standard error of the mean.

There are also some differences in the topological defects between the gel and the sol components of the system. Generally, the gel makes up 90% or more of the system. The sol in the heterogeneous networks had more first and second-order loops and less higher-order loops. In the homogeneous gels, the sol had more first-order loops and less higher-order loops. The fraction of truly fully cross-linked cross-linkers n_f is also shown, where first-order loops and dangling ends are not counted toward the degree of cross-linking, since they do not lead to connections to the surrounding network. Interestingly, the trend of n_f with heterogeneity ρ_h is different for the homogeneous and heterogeneous networks, in the homogeneous networks n_f decreases with ρ_h, and in the heterogeneous gels, it increases. The reason for this trend is that heterogeneous networks overall have fewer loop defects as ρ_h increases. The sol for all networks had less truly fully cross-linked cross-linkers, where first-order loops l_1 and dangling ends do not count toward being fully cross-linked.

The phantom modulus can be calculated by considering that each chain is an ideal elastic spring of stiffness $\propto N^{-1}$. Replacing each strand with an ideal spring, the ground state can be determined numerically by applying a simultaneous energy balance on all cross-linkers[26,40] using FIRE[49] energy minimization. Representative examples of the resulting minimized networks are shown in Figure 4. From these reduced network structures, it is straightforward to calculate the topological factor Γ, and elastically active strands μ_{eff} and cross-linkers ν_{eff} by using the following definitions

$$\Gamma = \left\langle \frac{\vec{R}^2}{Mb^2} \right\rangle = \frac{1}{N_p} \sum_{i=1}^{N_p} \frac{\vec{R}_i^{\,2}}{Mb^2} \tag{5}$$

In addition to Γ, the energy minimization also allowed the determination of ν_{eff}, the number of elastically effective (active) strands per unit volume, which are the ones that retain a length larger than zero after energy minimization, meaning they carried the load in the network. The number density μ_{eff} of the elastically effective cross-links is then defined as the ones that connect at least two elastically effective strands.

As shown in Figure 5, spatially heterogeneous networks tend to have more elastically active strands μ_{eff} and cross-linkers ν_{eff}, despite having a lower topological factor Γ. This indicates that there are more individual strands $\vec{R}_i$ in the heterogeneous networks that have a nonzero length after minimization, but the overall sum of their lengths is still lower than in the homogeneous networks. In the Supporting Information, we show the distribution of minimized strand lengths.

From these topological quantities, moduli from various theories can be derived as[52] $G_{ANT} = \Gamma\nu kT$ for the ANT, $G_{ANM} = \nu kT$ for the classical affine network model (ANM), and $G_{PNM} = (1-2/f)\nu kT$ for the phantom network theory. These moduli are shown in Figure 6. To independently determine the modulus of the networks numerically, we applied a simple shear deformation of $\gamma = 0.2$ to the fully reacted, equilibrated, and swollen gels in a MD simulation and measured the relaxation of the corresponding off-diagonal stress component τ_{xy}. After the initial decay, the steady-state value can be used to determine the modulus as $G_{num} = \tau_{xy}/\gamma$. This numerical result is plotted along with the theory estimates in Figure 6.

The homogeneous networks with topological defects followed the predictions of the ANT G_{ANT}, even though the networks contain defects and are swollen. This highlights the

https://doi.org/10.1021/acsengineeringau.3c00072
ACS Eng. Au 2024, 4, 351−358

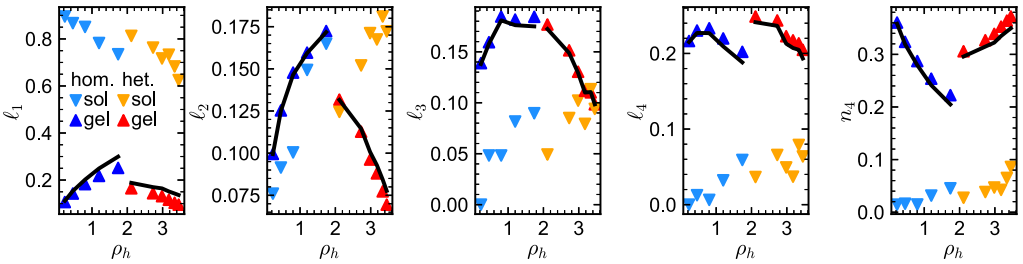

Figure 3. First-, second-, third-, and fourth-order loop fractions l_i, and fraction of truly fully cross-linked cross-linker n_4 in the sol and the gel as a function of ρ_h for homogeneous (blue, light blue) and heterogeneous (red, orange) fully reacted networks. The black lines indicate the values in the entire system. Each point is an average of 30 independent runs.

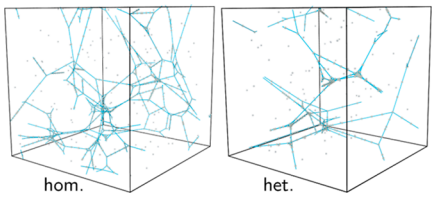

Figure 4. Representative snapshots of minimized fully reacted network structures of the systems with the highest respective heterogeneity ρ_h of 1.74 (hom.) and 3.45 (het.), where only the elastically effective strands are shown as straight connections in light blue. Note that the isolated cross-linkers are not unreacted, but are bonded by noneffective strands. Dense regions in these minimized structures contain many cross-linkers. The left shows the most dilute homogeneous case, and the right snapshot shows the most heterogeneous case.

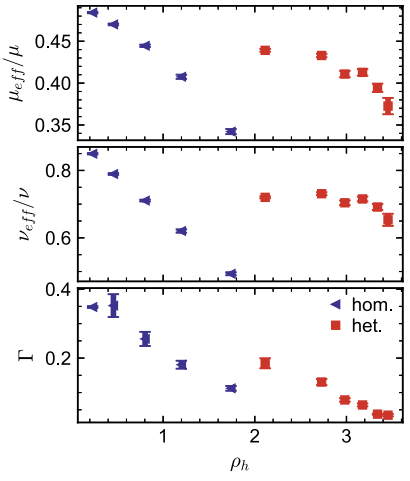

Figure 5. Elastically active cross-linkers μ_{eff}, elastically active strands ν_{eff}, and topological factor Γ, as a function of ρ_h for homogeneous (blue) and heterogeneous (red) systems. The theoretical values for ν_{eff} and μ_{eff} are 1 and $2/f$ respectively. Each point is an average of 30 independent fully reacted networks and the error bars indicate the standard error of the mean.

fact that the numerical measurement did estimate the near-equilibrium modulus. Previous work[40,53] also found good agreement of G_{ANT} and G_{num}. The topological factor Γ, therefore, does contain many of the nonideal effects caused by the topological defects. However, the spatially heterogeneous networks containing dense clusters did not follow any theoretical prediction. For the lowest spatial heterogeneity, the numerically determined modulus agrees with G_{ANT} but quickly departed from that prediction. For the higher spatial heterogeneity, ρ_h values, G_{num} approaches G_{PNM}. Interestingly,

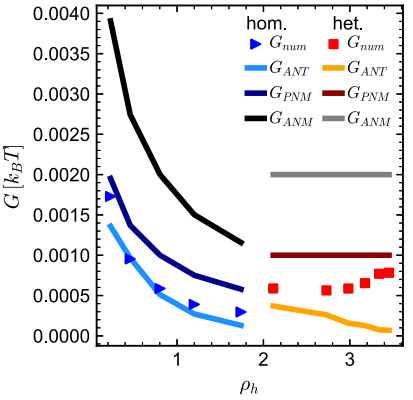

Figure 6. Moduli for homogeneous (blue) and heterogeneous (red) networks. Lines show results for affine network theory (ANT), affine network model (ANM), and phantom network theory (PNM).

the heterogeneous networks have higher shear moduli than the homogeneous gels, with some spatial heterogeneity. Additionally, the modulus of the heterogeneous networks is increasing with ρ_h, whereas all theories predict either a constant or a decreasing modulus. This trend is similar to the trend observed in ref 54. where they compared moduli as a function of density. This observation can be rationalized by the fact that the spatially heterogeneous network can be viewed as an effectively less dense gel, with small highly cross-linked dense regions. These dense regions did contribute more than theoretically expected by G_{ANT} to the elasticity, which led to an increased stiffness.

To investigate the mechanical behavior further, we performed extensional deformations of the fully reacted and equilibrated gels using MD simulations with breakable quartic bonds. The resulting stress–strain curves are displayed in Figure 7. Derived from these stress–strain curves, the maximum stress and maximum extension the gel networks exhibit were similar for both spatially and topologically defective networks, as shown in Figure 8. The maximum stress τ_{max} (the peak value in the stress–strain curve) decayed with increasing ρ_h for both network types, and the maximum extension λ_{max} (highest extension before the network breaks completely) decreased almost linearly with ρ_h. Both of these trends are expected, meaning all gels sustained less stress and broke earlier as ρ_h increased. The extension at which the maximum occurs, λ at τ_{max}, first increases with ρ_h, but then decreases for a high ρ_h. Additionally, there are noticeable small differences: both λ_{max} and λ at τ_{max} are slightly lower for the spatially heterogeneous networks.

Overall, the numerical moduli and deformation results led to the conclusion that even though spatially heterogeneous

https://doi.org/10.1021/acsengineeringau.3c00072
ACS Eng. Au 2024, 4, 351–358

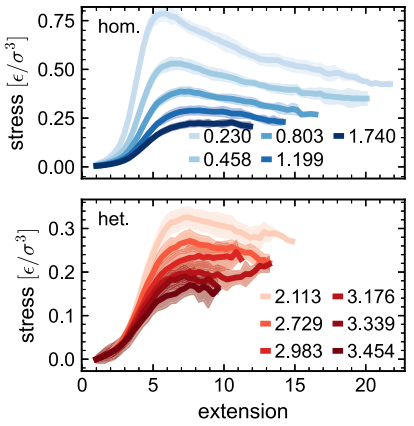

Figure 7. Stress τ vs extension λ curves for all fully formed gels. The legend indicates ρ_h values, and each line is averaged over 30 independent networks and the shaded area indicates the standard error of the mean.

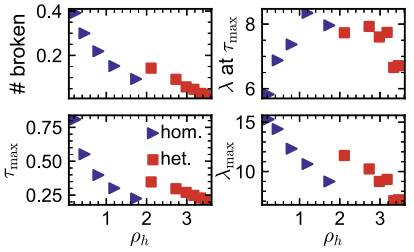

Figure 8. Maximum stress τ_{max}, maximum extension λ_{max}, extension λ at maximum stress τ_{max}, and the fraction of broken bonds as a function of ρ_h for homogeneous (blue) and heterogeneous (red) networks. Error bars are of the order of symbol size.

networks had fewer topological defects, they were less strong, i.e., slightly lower maximum stress and lower maximal extension, than corresponding spatially homogeneous networks with more topological defects. The heterogeneous gels were also stiffer, as indicated by a higher shear modulus. Interestingly, our observations are in agreement with bulk fracture theories,[31,55,56] where spatial heterogeneity is generally not incorporated.

Interestingly, in the spatially heterogeneous networks, we noted that fewer bonds need to be broken for the entire network to break under deformation, as illustrated in Figure 8a. This can be explained by the network structure, where only a few "key" strands connect the dense, highly cross-linked regions across much more dilute regions. Consequently, less strands need to be broken for the entire network to break. To illustrate this, a representative graph network structure is shown in Figure 9. Here, each strand was represented as an edge in a graph, and each cross-linker functioned as a node. Visually, strands that were between highly cross-linked regions were the ones that were more likely to break; broken bonds are indicated by dashed red lines in Figure 9. These observations also point toward the same interpretation as for the shear modulus, the spatially heterogeneous gels can be essentially viewed as networks with lower density and the small highly cross-linked dense regions contribute little to the mechanical properties.

To quantify this observation further, we determined strand properties as a function of whether they are broken or not, as shown in Figure 10. There are significant differences in the

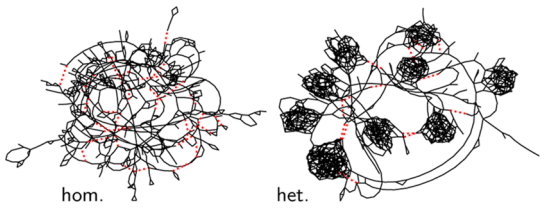

Figure 9. Graph network structures of the largest cluster, i.e. the gel, where loops and dangling ends are not shown. The left shows an example of the most homogeneous dilute case, and the right shows an example of the most heterogeneous case. Bonds that break during deformation are highlighted as red dashed lines.

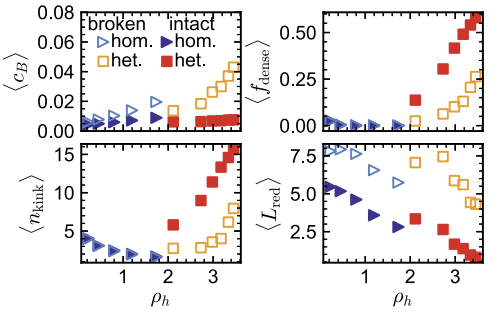

Figure 10. Average number of kinks, n_{kink}, reduced length, L_{red}, betweenness, c_B, and fraction of strands in the dense region, f_{dense}, for broken (open symbols) and not broken (filled symbols) bonds in the homogeneous (blue, light blue) and heterogeneous (red, orange) systems as a function of ρ_h.

properties of the broken and intact bonds. The heterogeneous networks have a substantially higher number of kinks n_{kink} (as determined by the geometry reduction algorithm Z_1[57,58]), indicating a much higher degree of entanglements. Additionally, the bonds that are broken (open symbols in Figure 10), have less kinks. The broken bonds were, on average, also in the less dense regions. In the homogeneous case, there was no difference in the number of kinks or local density for broken or intact bonds, and both are very low, to begin with. In both homogeneous and heterogeneous networks, the broken bonds had a higher value of betweenness[59,60] c_B, a network connectivity measure. In short, it quantifies the number of shortest paths in the entire graph that pass through a strand/edge; higher values indicate a more "important" strand connection that sits between more nodes. However, the difference between broken and intact betweenness values c_B was much more pronounced in the heterogeneous gels. In all networks, the broken bonds had significantly higher reduced lengths L_{red} in the initial configurations, as determined by energy minimization.

4. CONCLUSIONS

Spatial heterogeneity e.g., concentration fluctuations, and topological defects e.g., loops, are both important for properties of gels due to the different imprints they leave on the network structure. We present a simple extension to a network generation algorithm,[40,41] which enabled the investigation of the effect of spatial heterogeneities and topological defects on network properties. Both loop defects and spatial heterogeneity had different effects on the network properties.

Heterogeneous gels break at lower extensions than spatially homogeneous gels and sustain slightly lower maximum stresses, even though spatially heterogeneous networks have

https://doi.org/10.1021/acsengineeringau.3c00072
ACS Eng. Au 2024, 4, 351−358

more elastically active strands and cross-linkers. Despite having a lower topological factor, the shear moduli of heterogeneous networks were slightly higher than those of the homogeneous gels. Additionally, heterogeneous gels showed behavior deviating from theoretical predictions, whereas ANT predicts the shear moduli of homogeneous networks well.

Spatial heterogeneity also decreased the number of bonds that needed to be broken in order to break the entire gel. Additionally, broken bonds in heterogeneous networks had more distinct properties, such as having fewer kinks, being in the low-density region, and having higher betweenness values.

While the algorithm provided a simple and efficient way to generate networks with controlled topological defects and spatial heterogeneities, it also introduced some systematic effects that warrant further investigation. The sequential addition of strands introduces systematic effects that will become important when investigating properties during gel formation, e.g. gel points, and not just network properties of the fully formed networks as done here. Overall, the precise morphology and parameters of the spatial heterogeneity as small spherical dense clusters are somewhat arbitrary and artificial. Future careful evaluation and investigation of different types of spatial heterogeneities at different length scales will be needed.

Overall, simulations need to move toward more realistic gel structures to carefully detangle the effect of different types of defects. By providing a detailed analysis of the network structure and mechanical properties, our study highlighted the importance of considering both spatial and topological factors in understanding gel networks. In the future, investigating the connection between the microscopic molecular picture presented here and the macroscopic bulk fracture theories will be interesting. In addition, explicit solvent swelling simulations and comparisons to Flory−Rehner theory can be used to show the effects of the elastic contribution to swelling, as it is expected to be different due to differences in moduli. Other interesting future avenues include the effects of heterogeneities on glass transition temperatures,[61,62] where the density fluctuations in particular are expected to have an effect on segmental mobility.

■ ASSOCIATED CONTENT

Supporting Information

The Supporting Information is available free of charge at https://pubs.acs.org/doi/10.1021/acsengineeringau.3c00072.

> Details on the monomer pair interactions, code, and explanation for generating the cross-linker distribution, gel points and devulcanization data, loops during cross-linking, quantification of higher-order loops and topological defects, strand length distributions, local density distributions, second virial coefficient, and swelling ratios of the gels (PDF)

■ AUTHOR INFORMATION

Corresponding Author

Antonia Statt − *Materials Science and Engineering, Grainger College of Engineering, University of Illinois, Urbana-Champaign, Champaign, Illinois 61801, United States;* orcid.org/0000-0002-6120-5072; Email: statt@illinois.edu

Author

B. Ruşen Argun − *Mechanical Engineering, Grainger College of Engineering, University of Illinois, Urbana-Champaign, Champaign, Illinois 61801, United States*

Complete contact information is available at: https://pubs.acs.org/10.1021/acsengineeringau.3c00072

Author Contributions

CRediT: **B. Ruşen Argun** data curation, investigation, methodology, validation, writing-review & editing; **Antonia Statt** conceptualization, formal analysis, funding acquisition, investigation, methodology, project administration, resources, supervision, visualization, writing-original draft, writing-review & editing.

Notes

The authors declare no competing financial interest.

■ ACKNOWLEDGMENTS

The authors thank C.E. Sing, J.E. Laaser, and A.S. Kuenstler for insightful discussions and careful reading of this manuscript. The authors acknowledge the Molecule Maker Lab Institute (MMLI), supported by NSF under award no. 2019897.

■ REFERENCES

(1) Gu, Y.; Zhao, J.; Johnson, J. A. Polymer Networks: From Plastics and Gels to Porous Frameworks. *Angew. Chem., Int. Ed.* **2020**, *59*, 5022−5049.

(2) Creton, C. 50th anniversary perspective: Networks and gels: Soft but dynamic and tough. *Macromolecules* **2017**, *50*, 8297−8316.

(3) Van Vlierberghe, S.; Dubruel, P.; Schacht, E. Biopolymer-based hydrogels as scaffolds for tissue engineering applications: a review. *Biomacromolecules* **2011**, *12*, 1387−1408.

(4) Koetting, M. C.; Peters, J. T.; Steichen, S. D.; Peppas, N. A. Stimulus-responsive hydrogels: Theory, modern advances, and applications. *Mater. Sci. Eng.: R: Rep.* **2015**, *93*, 1−49.

(5) Lubensky, T.; Isaacson, J. Field theory for the statistics of branched polymers, gelation, and vulcanization. *Phys. Rev. Lett.* **1978**, *41*, 829−832.

(6) Macosko, C. W.; Miller, D. R. A new derivation of average molecular weights of nonlinear polymers. *Macromolecules* **1976**, *9*, 199−206.

(7) Miller, D. R.; Macosko, C. W. A new derivation of postgel properties of network polymers. *Rubber Chem. Technol.* **1976**, *49*, 1219−1231.

(8) Christensen, K. *Percolation Theory*; Imperial College London, 2002; Vol. *1*.

(9) Ahmad, Z.; Stepto, R. F. T. Approximate theories of gelation. *Colloid Polym. Sci.* **1980**, *258*, 663−674.

(10) Witten, T. A.; Sander, L. M. Diffusion-limited aggregation. *Phys. Rev. B* **1983**, *27*, 5686−5697.

(11) Miller, D. R.; Macosko, C. W. A New Derivation of Post Gel Properties of Network Polymers. *Macromolecules* **1976**, *9*, 206−211.

(12) Flory, P. J. Molecular size distribution in three dimensional polymers. i. gelation1. *J. Am. Chem. Soc.* **1941**, *63*, 3083−3090.

(13) Stockmayer, W. H. Theory of molecular size distribution and gel formation in branched-chain polymers. *J. Chem. Phys.* **1943**, *11*, 45−55.

(14) Tang, Z.; Jiang, L. Visualization of single crosslinks and heterogeneity in polymer networks. *Giant* **2022**, *12*, 100131.

(15) Furuya, T.; Koga, T. Molecular simulation of polymer gels synthesized by free radical copolymerization: Effects of concentrations and reaction rates on structure and mechanical properties. *Polymer* **2023**, *279*, 126012.

(16) Rudyak, V. Y.; Kozhunova, E. Y.; Chertovich, A. V. Towards the realistic computer model of precipitation polymerization microgels. *Sci. Rep.* **2019**, *9*, 13052.
(17) Gu, Y.; Zhao, J.; Johnson, J. A. A (macro) molecular-level understanding of polymer network topology. *Trends Chem.* **2019**, *1*, 318−334.
(18) Dookhith, A. Z.; Lynd, N. A.; Creton, C.; Sanoja, G. E. Controlling architecture and mechanical properties of polyether networks with organoaluminum catalysts. *Macromolecules* **2022**, *55*, 5601−5609.
(19) Cuthbert, J.; Wanasinghe, S. V.; Matyjaszewski, K.; Konkolewicz, D. Are raft and atrp universally interchangeable polymerization methods in network formation? *Macromolecules* **2021**, *54*, 8331−8340.
(20) Li, X.; Nakagawa, S.; Tsuji, Y.; Watanabe, N.; Shibayama, M. Polymer gel with a flexible and highly ordered three-dimensional network synthesized via bond percolation. *Sci. Adv.* **2019**, *5*, No. eaax8647.
(21) Danielsen, S. P. O.; Beech, H. K.; Wang, S.; El-Zaatari, B. M.; Wang, X.; Sapir, L.; Ouchi, T.; Wang, Z.; Johnson, P. N.; Hu, Y.; et al. Molecular characterization of polymer networks. *Chem. Rev.* **2021**, *121*, 5042−5092.
(22) Asai, M.; Katashima, T.; Chung, U.-i.; Sakai, T.; Shibayama, M. Correlation between local and global inhomogeneities of chemical gels. *Macromolecules* **2013**, *46*, 9772−9781.
(23) Di Lorenzo, F.; Seiffert, S. Nanostructural heterogeneity in polymer networks and gels. *Polym. Chem.* **2015**, *6*, 5515−5528.
(24) Wang, R.; Lin, T.-S.; Johnson, J. A.; Olsen, B. D. Kinetic Monte Carlo Simulation for Quantification of the Gel Point of Polymer Networks. *ACS Macro Lett.* **2017**, *6*, 1414−1419.
(25) Alamé, G.; Brassart, L. Effect of topological defects on the elasticity of near-ideal polymer networks. *J. Appl. Mech.* **2020**, *87*, 121006.
(26) Lang, M.; Müller, T. Analysis of the Gel Point of Polymer Model Networks by Computer Simulations. *Macromolecules* **2020**, *53*, 498−512.
(27) Arora, A.; Lin, T.-S.; Olsen, B. D. Coarse-grained simulations for fracture of polymer networks: Stress versus topological inhomogeneities. *Macromolecules* **2022**, *55*, 4−14.
(28) Martín-Molina, A.; Quesada-Pérez, M. A review of coarse-grained simulations of nanogel and microgel particles. *J. Mol. Liq.* **2019**, *280*, 374−381.
(29) Quesada-Pérez, M.; Martín-Molina, A. Solute diffusion in gels: thirty years of simulations. *Adv. Colloid Interface Sci.* **2021**, *287*, 102320.
(30) Slootman, J.; Waltz, V.; Yeh, C. J.; Baumann, C.; Göstl, R.; Comtet, J.; Creton, C. Quantifying rate-and temperature-dependent molecular damage in elastomer fracture. *Phys. Rev. X* **2020**, *10*, 041045.
(31) Creton, C.; Ciccotti, M. Fracture and adhesion of soft materials: a review. *Rep. Prog. Phys.* **2016**, *79*, 046601.
(32) Rebello, N. J.; Beech, H. K.; Olsen, B. D. Adding the effect of topological defects to the Flory−Rehner and Bray−Merrill swelling theories. *ACS Macro Lett.* **2021**, *10*, 531−537.
(33) Zhong, M.; Wang, R.; Kawamoto, K.; Olsen, B. D.; Johnson, J. A. Quantifying the impact of molecular defects on polymer network elasticity. *Science* **2016**, *353*, 1264−1268.
(34) Shen, J.; Lin, X.; Liu, J.; Li, X. Effects of Cross-Link Density and Distribution on Static and Dynamic Properties of Chemically Cross-Linked Polymers. *Macromolecules* **2019**, *52*, 121−134.
(35) Furuya, T.; Koga, T. Effects of Primary Structure of Reactive Polymers on Network Structure and Mechanical Properties of Gels. *Macromol. Theory Simul.* **2022**, *31*, 2200044.
(36) Lei, J.; Xu, S.; Li, Z.; Liu, Z. Study on large deformation behavior of polyacrylamide hydrogel using dissipative particle dynamics. *Front. Chem.* **2020**, *8*, 115.
(37) Sliozberg, Y. R.; Hoy, R. S.; Mrozek, R. A.; Lenhart, J. L.; Andzelm, J. W. Role of entanglements and bond scission in high strain-rate deformation of polymer gels. *Polymer* **2014**, *55*, 2543−2551.
(38) Rottach, D. R.; Curro, J. G.; Budzien, J.; Grest, G. S.; Svaneborg, C.; Everaers, R. Permanent set of cross-linking networks: Comparison of theory with molecular dynamics simulations. *Macromolecules* **2006**, *39*, 5521−5530.
(39) Furuya, T.; Koga, T. Molecular simulation of networks formed by end-linking of tetra-arm star polymers: Effects of network structures on mechanical properties. *Polymer* **2020**, *189*, 122195.
(40) Gusev, A. A. Numerical Estimates of the Topological Effects in the Elasticity of Gaussian Polymer Networks and Their Exact Theoretical Description. *Macromolecules* **2019**, *52*, 3244−3251.
(41) Gusev, A. A.; Schwarz, F. Molecular Dynamics Validation and Applications of the Maximum Entropy Homogenization Procedure for Predicting the Elastic Properties of Gaussian Polymer Networks. *Macromolecules* **2019**, *52*, 9445−9455.
(42) Wang, S.; Ramkrishna, D.; Narsimhan, V. Exact sampling of polymer conformations using Brownian bridges. *J. Chem. Phys.* **2020**, *153*, 034901.
(43) Arora, A.; Lin, T.-S.; Olsen, B. D. Coarse-Grained Simulations for Fracture of Polymer Networks: Stress Versus Topological Inhomogeneities. *Macromolecules* **2022**, *55*, 4−14.
(44) Kremer, K.; Grest, G. S. Dynamics of entangled linear polymer melts: A molecular-dynamics simulation. *J. Chem. Phys.* **1990**, *92*, 5057−5086.
(45) Warner, H. R., Jr Kinetic theory and rheology of dilute suspensions of finitely extendible dumbbells. *Ind. Eng. Chem. Fundam.* **1972**, *11*, 379−387.
(46) Weeks, J. D.; Chandler, D.; Andersen, H. C. Role of repulsive forces in determining the equilibrium structure of simple liquids. *J. Chem. Phys.* **1971**, *54*, 5237−5247.
(47) Rottler, J.; Robbins, M. O. Growth, microstructure, and failure of crazes in glassy polymers. *Phys. Rev. E* **2003**, *68*, 011801.
(48) Wang, J.; Ge, T. Crazing reveals an entanglement network in glassy ring polymers. *Macromolecules* **2021**, *54*, 7500−7511.
(49) Bitzek, E.; Koskinen, P.; Gähler, F.; Moseler, M.; Gumbsch, P. Structural relaxation made simple. *Phys. Rev. Lett.* **2006**, *97*, 170201.
(50) Anderson, J. A.; Glaser, J.; Glotzer, S. C. HOOMD-blue: A Python package for high-performance molecular dynamics and hard particle Monte Carlo simulations. *Comput. Mater. Sci.* **2020**, *173*, 109363.
(51) Howard, M. P.; Statt, A.; Madutsa, F.; Truskett, T. M.; Panagiotopoulos, A. Z. Quantized bounding volume hierarchies for neighbor search in molecular simulations on graphics processing units. *Comput. Mater. Sci.* **2019**, *164*, 139−146.
(52) Panyukov, S. Theory of flexible polymer networks: Elasticity and heterogeneities. *Polymers* **2020**, *12*, 767.
(53) Gusev, A. A.; Schwarz, F. Molecular Dynamics Study on the Validity of Miller-Macosko Theory for Entanglement and Crosslink Contributions to the Elastic Modulus of End-Linked Polymer Networks. *Macromolecules* **2022**, *55*, 8372−8383.
(54) Akagi, Y.; Gong, J. P.; Chung, U.-i.; Sakai, T. Transition between phantom and affine network model observed in polymer gels with controlled network structure. *Macromolecules* **2013**, *46*, 1035−1040.
(55) Spagnoli, A.; Brighenti, R.; Cosma, M. P.; Terzano, M. Fracture in soft elastic materials: Continuum description, molecular aspects and applications. *Adv. Appl. Mech.* **2022**, *55*, 255−307.
(56) Long, R.; Hui, C.-Y.; Gong, J. P.; Bouchbinder, E. The fracture of highly deformable soft materials: A tale of two length scales. *Annu. Rev. Condens. Matter Phys.* **2021**, *12*, 71−94.
(57) Kröger, M. Shortest multiple disconnected path for the analysis of entanglements in two-and three-dimensional polymeric systems. *Comput. Phys. Commun.* **2005**, *168*, 209−232.
(58) Kröger, M.; Dietz, J. D.; Hoy, R. S.; Luap, C. The z1 + package: Shortest multiple disconnected path for the analysis of entanglements in macromolecular systems. *Comput. Phys. Commun.* **2023**, *283*, 108567.

https://doi.org/10.1021/acsengineeringau.3c00072
ACS Eng. Au 2024, 4, 351−358

(59) Brandes, U. A faster algorithm for betweenness centrality. *J. Math. Sociol.* **2001**, *25*, 163−177.
(60) Brandes, U. On variants of shortest-path betweenness centrality and their generic computation. *Social Networks* **2008**, *30*, 136−145.
(61) Nie, W.; Douglas, J. F.; Xia, W. Competing effects of molecular additives and cross-link density on the segmental dynamics and mechanical properties of cross-linked polymers. *ACS Eng. Au* **2023**, *3*, 512−526.
(62) Lin, T.-W.; Mei, B.; Schweizer, K. S.; Sing, C. E. Simulation study of the effects of polymer network dynamics and mesh confinement on the diffusion and structural relaxation of penetrants. *J. Chem. Phys.* **2023**, *159*, 014904.

https://doi.org/10.1021/acsengineeringau.3c00072
ACS Eng. Au 2024, 4, 351−358